Disentangling fractional momentum transfer in the ^{19}F + ^{154}Sm system

Amritraj Mahato ◉, Dharmendra Singh ◉,* Nitin Sharma, Pankaj K. Giri, and Sneha B. Linda
Department of Physics, Central University of Jharkhand, Ranchi 835222, India

Harish Kumar, Suhail A. Tali ◉, Asif Ali, and M. Afzal Ansari
Department of Physics, Aligarh Muslim University, Aligarh 202002, India

Nabendu Kumar Deb ◉
Department of Physics, Gauhati University, Guwahati, Assam 781014, India

N. P. M. Sathik
Department of Physics, Jamal Mohamed College, Tiruchirappalli 620020, India

S. Kumar, R. Kumar, S. Muralithar, and R. P. Singh
Inter University Accelerator Centre, Aruna Asaf Ali Marg, New Delhi 110067, India

Forward recoil range distributions of evaporation residues produced in the system ^{19}F + ^{154}Sm were measured at projectile energy $\approx$107 MeV using the offline γ-ray activation technique. The entire and fractional linear momentum transfers inferred from these recoil range distributions were used to identify the evaporation residues formed by complete and incomplete fusion mechanisms. The forward recoil range distributions of measured evaporation residues populated through xn/pxn channels were found to be consisting of a single peak only while the evaporation residues populated through α emitting channel had contributions from incomplete fusion also. The observed incomplete fusion process in the population of α emitting channel residues is explained through the breakup fusion model. The results indicate the occurrence of incomplete fusion involving the breakup of ^{19}F into ^{4}He + ^{15}N and/or ^{8}Be + ^{11}B followed by fusion of one of the fragments with target nucleus ^{154}Sm. From these measurements, the relative contributions of complete and incomplete fusion were separated out. The forward recoil range distributions data show that the incomplete fusion contribution in the fusion of fragment ^{15}N is more dominant as compared to the fusion of fragment ^{11}B with ^{154}Sm target due to the smaller value of α breakup threshold energy ($E_{\mathrm{B.U.}}^{\alpha}$). The measured forward recoil range distributions of evaporation residues produced through α emitting channels provide experimental signature of strong clustering in ^{19}F projectile as α and ^{15}N. The incomplete fusion strength function has also been deduced from the measured recoil range distributions and found to be compatible with those deduced from the measured excitation functions for the same system and beam energy.

I. INTRODUCTION

The mechanisms of heavy-ion nuclear reactions on medium-mass targets have been studied for many years. The dominant process is generally complete fusion (CF), in which the incident projectile completely amalgamates with the target nucleus, forming an excited compound nucleus from which particles are subsequently evaporated. However, it has become increasingly apparent that in many cases there are significant contributions from incomplete-fusion (ICF) processes, in which only part of the projectile fuses with the target nucleus to give an excited intermediate composite system [1]. The role of deformation in heavy-ion fusion is important in understanding the fusion dynamics [2,3]. The fusion barrier distributions

are influenced by deformation in fusion reactions involving deformed nuclei [4,5]. The fusion of light deformed projectile nuclei with a heavy collision partner modifies the fusion barrier distribution, which hinders the sub-barrier fusion cross section [6]. The influence of hexadecapole deformation on production cross sections of superheavy nuclei are also studied in the literature [7]. It has also been observed that the fusion barriers are reduced by induced nuclear deformations [8]. The influence of nuclear deformation on the fusion mechanism has been the object of various investigations, including the fusion barrier distribution [4,9]. The nuclear deformation may initiate the quasifission, thereby inhibiting fusion [4]. Nuclear shapes and deformation influences quasifission and fusion-fission process. It has been observed that the collisions with the tips of the deformed target nucleus lead to quasifission. However, collisions with the sides of the deformed target nucleus lead to fusion-fission [10,11]. Entrance
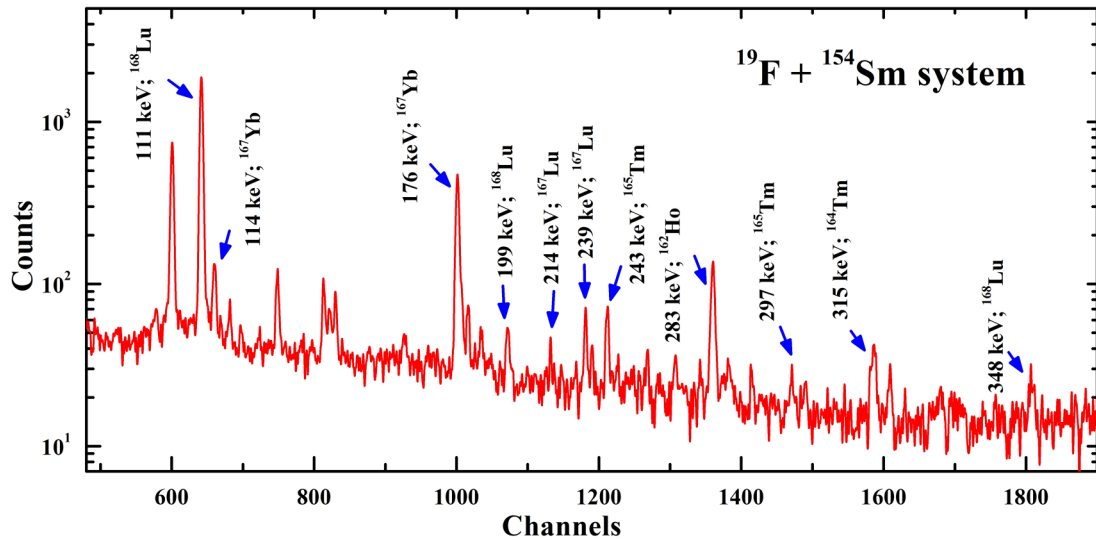
*dsinghcuj@gmail.com

FIG. 1. Typical γ-ray spectrum of the FRRDs (cumulative thickness ≈ 0.676 mg/cm^2) of residues populated in the ^{19}F + ^{154}Sm system at $E_{\text{Lab}} \approx 107$ MeV, recorded for about 600 s and 20 min after the ending of irradiation of stack using HPGe γ-ray spectrometer.

channel effects plays important role in the heavy-ion fusion mechanism. It is observed that Coulomb interaction parameter suppress the heavy-ion fusion [12]. Any single entrance channel parameter may not be able to explain the fusion mechanism completely [13]. Therefore, a combination of channel parameters and/or a parameter which can incorporate all gross features of interacting partners should be chosen to study the systematics of the heavy-ion reaction [14]. Charge asymmetry also influences the heavy-ion fusion [15]. The fusion probability is also found to increase with entrance channel mass asymmetry of the projectile-target systems [16–18]. Many attempts were available on the dependence of entrance channel effects such as projectile energy, projectile structure, target charge, mass asymmetry, $Z_P Z_T$, etc., using different projectile-target combinations [16–21]. A systematic of the deformation of target on the ICF probability is also available in literature [22].

^{19}F has been the subject of many investigations, focusing on the study of cluster structures in $N \neq Z$ nuclei [23,24]. In these systems, exotic cluster configurations may show up, having chemical bonding like structures. The ^{19}F excitation energy spectrum has been analyzed using microscopic and semimicroscopic models as well as phenomenological potential models [25,26]. Essentially, ^{19}F can be described as a one-proton-deficient system of ^{19}Ne, and thus the level sequence has been interpreted by considering the α-hole cluster model as well as the coupling of the $\alpha + {}^{15}$N channel [27,28]. It is also worth mentioning the recent work [29], addressing the occurrence of α clustering in the ^{19}Ne mirror nucleus. The study of $\alpha + {}^{15}$N scattering can help us to better constrain the spectroscopy of ^{19}Ne [30].

The present work extends this approach to the entrance channel ^{19}F + ^{154}Sm to get an experimental evidence of the occurrence of incomplete fusion. The forward recoil range distributions (FRRDs) for the evaporation residues (ERs) populated through CF and/or ICF in the same system at projectile energy (E_{Lab}) ≈ 107 MeV were measured. The recoil ranges

measured in this work are projected ranges along the beam direction and do not reveal any angular dependence of cross sections and velocities of the ERs. The relative contributions of CF and ICF have also been deduced from the measured recoil range distributions data. The present paper is organized as follows: The experimental techniques are given in Sec. II, interpretation of the measured results are discussed in Sec. III, and the summary and conclusions of the present study are given in Sec. IV.

II. EXPERIMENTAL TECHNIQUES USED FOR FORWARD RECOIL RANGE DISTRIBUTIONS

The present experiment was performed using 15 UD Pelletron at Inter University Accelerator Centre (IUAC), New Delhi, India. The FRRDs of ERs were measured by bombarding ^{19}F beam of $E_{\text{Lab}} \approx 107$ MeV on ^{154}Sm target backed by a stack of thin aluminium (Al) catcher foils. The isotopically enriched ^{154}Sm target (enrichment $\approx 98.4\%$) of thickness ≈ 0.3 mg/cm^2 was prepared by vacuum evaporation technique in target fabrication laboratory at IUAC, New Delhi, India [31]. The target was mounted with the ^{154}Sm layer downstream and followed immediately by a stack of 26 thin evaporated aluminium catcher foils, each having thickness between 30 and 100 μg/cm^2. The thickness of each catcher foil was determined prior to its use, by measuring the energy lost by 5.8 MeV α particles from a ^{241}Am source in traversing the foil as well as Rutherford back scattering technique [32]. The weighted average beam current of ≈ 15 nA was measured behind the target assembly with an electron suppressed Faraday cup, using a current integrator device. Keeping in view the half-lives of interest, irradiations have been carried out for about 11 h duration. The beam fluxes measured by two methods (time weighted beam current and total charge collected in Faraday cup) were found to agree with each other within a 10% variation. The mean energy of the ^{19}F-ion beam incident at half the thickness on each
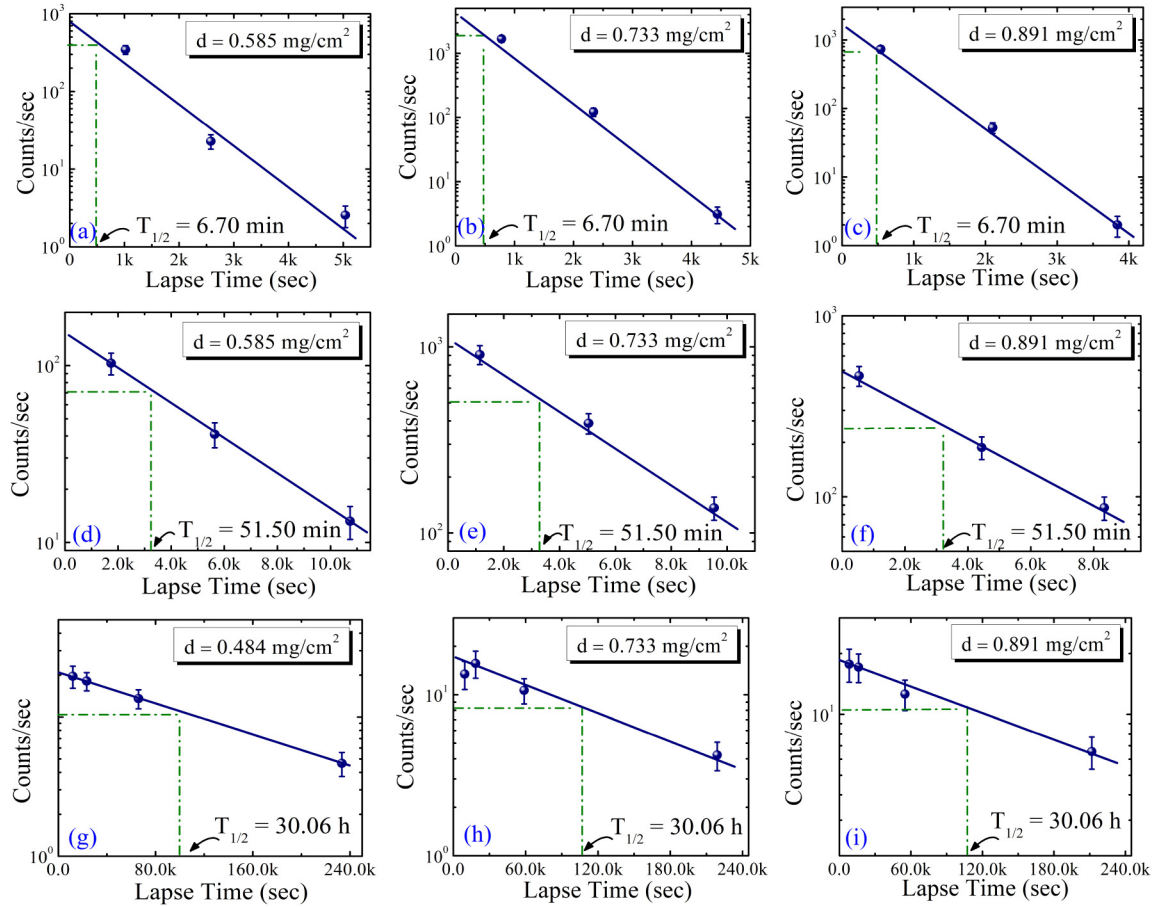
FIG. 2. The decay curves of some measured residues ^{168}Lu ($T_{1/2} = 6.70$ min; $E_\gamma = 199$ keV, $B_R = 28.0\%$), ^{167}Lu ($T_{1/2} = 51.50$ min; $E_\gamma = 239$ keV, $B_R = 8.6\%$), and ^{165}Tm ($T_{1/2} = 30.06$ h; $E_\gamma = 243$ keV, $B_R = 35.5\%$) corresponding to three different cumulative catcher thicknesses of aluminium.

foil in the stack was calculated from the energy degradation of the incident beam energy, using stopping power and range software SRIM [33]. The inherent energy spread in 107 MeV ^{19}F beam is found to be 600 keV. When the beam passes through the target, the energy spread due to straggling may come into picture. However, the energy spread due to straggling has not been considered due to its insignificant contribution [34].

After the irradiation, the stack of Al catchers along with ^{154}Sm target was taken out from the scattering chamber using In Vacuum Transfer Facility. The target-catcher assembly was dismantled to record the activities induced in the individual irradiated catcher foil. The activities induced in each Al catcher was recorded individually at increasing time intervals using precalibrated high-resolution high-purity germanium (HPGe) γ-ray spectrometer coupled to a CAMAC-based personal computer employing CANDLE software [35]. The HPGe γ-ray spectrometer (resolution 2 keV for a 1.408-MeV γ ray of ^{152}Eu) was calibrated for energy and efficiency. To determine the geometry-dependent efficiency of the HPGe detector at various source-detector distances, a standard source of ^{152}Eu of known strength was used. The induced activity in various Al catchers were used to measure the production probability of different ERs. The identification of ERs was done on the

basis of their characteristic γ rays and also by following their half-lives. Typical γ spectra recorded for the FRRDs (cumulative thickness ≈ 0.676 mg/cm^2) showing some of the identified γ peaks at energy ≈ 107 MeV is shown in Fig. 1. The decay curves of some measured residues ^{168}Lu ($T_{1/2} = 6.70$ min; $E_\gamma = 199$ keV, $B_R = 28.0\%$), ^{167}Lu ($T_{1/2} = 51.50$ min; $E_\gamma = 239$ keV, $B_R = 8.6\%$), and ^{165}Tm ($T_{1/2} = 30.06$ h; $E_\gamma = 243$ keV, $B_R = 35.5\%$) corresponding to three different cumulative catcher thicknesses of aluminium are shown in Fig. 2. The spectroscopic data used in the determination of production cross sections of various ERs were taken from Refs. [36,37]. A list of identified ERs produced via CF and/or ICF dynamics in ^{19}F $+$ ^{154}Sm system along with their decay characteristics, e.g., γ-ray energy (E_γ), and branching ratios (B_R) is given in Table I. The measured cross sections σ_{ER} for a particular ER were calculated using the standard formulation [38],

$$\sigma_{\text{ER}} = -\frac{A\lambda\exp(\lambda t_{\text{lps}})}{N_0\phi B_R k_{\text{sac}}\epsilon[1 - \exp(-\lambda t_{\text{ird}})][1 - \exp(-\lambda t_{\text{cnt}})]}$$

(1)

where A is the total number of counts in the photopeak recorded in irradiation time t_{ird}, λ is the decay constant of the residue, N_0 is the total number of target nuclei, B_R is the

TABLE I. Measured ERs produced via different reaction channels in the ^{19}F + ^{154}Sm system at $E_{\text{Lab}} \approx 107$ MeV along with their spectroscopic data [36,37].

S. No.	Reaction channels	Half-life	$E\gamma$ (keV)	B_R (%)
1.	^{154}Sm (F, 5n) ^{168}Lu	5.50 min (g)	111	49.00[a]
			228	7.00[a]
			348	6.70[a]
		6.70 min (m)	199	76.00[a]
			979	15.70[a]
			896	9.00[a]
			885	7.70[a]
2.	^{154}Sm (F, 6n) ^{167}Lu	51.50 min	239	8.60
			214	3.60
			179	2.80
3.	^{154}Sm (F, p5n) ^{167}Yb	17.50 min (m)	114	55.40
			176	21.00
4.	^{154}Sm (F, α3n) ^{166}Tm	7.70 h (m)	779	18.90
			183	16.10
			705	10.96
5.	^{154}Sm (F, α4n) ^{165}Tm	30.06 h	243	35.50
			297	12.71
6.	^{154}Sm (F, α5n) ^{164}Tm	5.10 min	208	14.60
			315	10.00
7.	^{154}Sm (F, 2α3n) ^{162}Ho	1.13 h	187	28.60
			283	11.30
8.	^{154}Sm (F, 2α4n) ^{161}Ho	2.48 h	211	46.00

[a]Relative intensity.

branching ratio of the identified γ ray, ϕ is the flux of the incident beam, ϵ is the geometry dependent efficiency of the HPGe detector, t_{lps} is the time elapsed between the stop of irradiation and start of the counting, t_{cnt} is the counting time, and $k_{\text{sac}} = [1 - e^{-\mu_c d}]/\mu_c d$ is the self-absorption correction factor for the target of thickness d with absorption coefficient μ_c. Further details regarding the experimental setup and cross section measurement can be found in Ref. [22].

The measured yields of an ER as a function of the range in stopping medium are associated with errors and uncertainties in the thickness of target and catcher foils, counting statistics, etc. Several factors are responsible for the uncertainties in the measured yields. The main factors are the following: (i) the uncertainty due to the nonuniformity of the target and thickness measurement was estimated to be less than 3%, (ii) the error arising from the fluctuations in beam current is estimated to be less than 6%, (iii) the uncertainty in the efficiency calibration of the HPGe detector was estimated to be less than 5%, (iv) to minimize the error, the counting was done for dead time below 10%, and (v) uncertainty due to the straggling effect of the projectile passing through the stack was estimated to be less than 2%. The overall uncertainties from various factors including statistical errors in the photopeak area are estimated to be less than 22%.

III. ANALYSIS AND RESULTS

In order to get a clear picture of the different fusion processes involved in the production of ERs in the ^{19}F + ^{154}Sm

system at $E_{\text{Lab}} \approx 107$ MeV, measurements of FRRDs of the observed residues were done. A total of eight ERs, namely, ^{168}Lu (5n), ^{167}Lu (6n), ^{167}Yb (p5n), ^{166}Tm (α3n), ^{165}Tm (α4n), ^{164}Tm (α5n), ^{162}Ho (2α3n), and ^{161}Ho (2α4n) were populated through CF and/or ICF channels in this measurement. Among the observed ERs, residues populated via α emission channels (^{166}Tm, ^{165}Tm, ^{164}Tm, ^{162}Ho, and ^{161}Ho) have the possibility of getting populated through the CF as well ICF processes. On the other hand, residues populated via xn/pxn channels (^{168}Lu, ^{167}Lu, and ^{167}Yb) are likely to get populated through the CF process only. Residues populated through CF and/or ICF processes undergo an intermediate stage, where an excited compound system is formed through the total or partial fusion of the incident projectile with the target nucleus. In CF process, the intermediate compound nucleus (CN) recoils along the direction of projectile with a velocity and excitation energy governed totally by the energy and momentum of the incident projectile, while in ICF process the intermediate composite system formed at a particular beam energy is populated with an extended distribution of recoil velocity, recoil angle, and excitation energy [39].

The technique of FRRDs is capable of providing detailed information about the reaction mechanism of different fusion processes involved in the population of ERs. The measurement of recoil velocity of the heavy products or, equivalently, its FRRD in a stopping medium, can be useful in determining the degree of linear momentum transfer (LMT) from the incident projectile to the resulting compound system. Careful measurement of FRRDs of the residues populated is a powerful tool for disentangling the different ICF processes, where the same product may get populated through multiple fusion processes, followed by different degrees of charged particle evaporation. The measured yields of the reaction products in each foil were divided by the thickness of respective foil (in mg/cm^2), to get the normalized yields of measured ERs. The projected FRRDs, thus reflects the velocity distribution of the populated ERs recoiling in the catcher medium. The normalized yields [mb/(mg/cm^2)] were then plotted against the cumulative catcher thickness to obtain the differential FRRDs.

Residues originate from an intermediate compound system recoil in the Al stopping medium with a well-defined velocity v$_0$. The velocity distribution of the reaction products is symmetric about v$_0$ with a width associated with the number of nucleons and/or α particles emitted by the recoiling intermediate compound system. For the CF process, the recoil velocity of the intermediate compound system v$_0$ derived from the conservation of linear momentum is given as

$$v_0 = V_{\text{CN}} = \frac{\sqrt{2m_p E_{\text{Lab}}}}{M_{\text{CN}}}, \tag{2}$$

where m_p and M_{CN} are the masses of incident projectile and intermediate compound system, respectively and E_{Lab} is the laboratory energy of the incident projectile. The recoil velocity of an incompletely fused compound (IFC) system formed through the ICF process will be less than v$_0$ since a fraction of the incident linear momentum p$_{\text{inc}}$ is carried

TABLE II. Measured most probable ranges deduced from FRRDs curves and theoretically calculated mean ranges for CF and ICF components (in mg/cm^2) produced in the ^{19}F + ^{154}Sm system at $E_{\text{Lab}} \approx 107$ MeV.

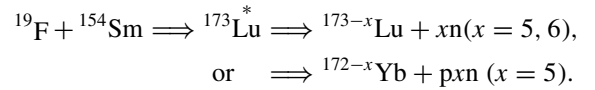| S. No	Reactions	CF		ICF-α		ICF-2α	
		R_{SRIM}	R_{Meas}	R_{SRIM}	R_{Meas}	R_{SRIM}	R_{Meas}
1.	^{154}Sm (F, 5n) ^{168}Lu	0.702	0.729 ± 0.085[a]	–	–	–	–
2.	^{154}Sm (F, 6n) ^{167}Lu	0.699	0.749 ± 0.079[a]	–	–	–	–
3.	^{154}Sm (F, p5n) ^{167}Yb	0.705	0.733 ± 0.064[a]	–	–	–	–
4.	^{154}Sm (F, α3n) ^{166}Tm	0.718	0.711 ± 0.087[a]	0.478	0.482 ± 0.062[a]	–	–
5.	^{154}Sm (F, α4n) ^{165}Tm	0.716	0.756 ± 0.092[a]	0.475	0.479 ± 0.073[a]	–	–
6.	^{154}Sm (F, α5n) ^{164}Tm	0.710	0.729 ± 0.071[a]	0.472	0.494 ± 0.066[a]	–	–
7.	^{154}Sm (F, 2α3n) ^{162}Ho	–	–	0.475	0.496 ± 0.066[a]	0.267	0.254 ± 0.057[a]
8.	^{154}Sm (F, 2α4n) ^{161}Ho	–	–	0.472	0.487 ± 0.088[a]	0.265	0.246 ± 0.055[a]

[a]Errors are the standard deviations

away by the spectator. Considering the projectile to be a point object, p_{inc} will be shared between the fusing fragment and spectator in a ratio proportional to their masses. Furthermore, since the diameter of the incident projectile is extended over a range of impact parameters and, the spectator generally breaks up from the outer region of the incident projectile, the linear momentum associated with the intermediate compound system, by a fusing fragment of mass m_f from an incident projectile of mass m_p and linear momentum p_{inc}, is equal to $(m_f/m_p).p_{\text{inc}}$.

Forward recoil ranges of the measured ERs were also calculated using the classical approach and the code SRIM [33]. Values of the calculated ranges (R_{SRIM}) of the ERs were found to agree well with the measured ones (R_{Meas}) tabulated in Table II.

A. FRRDs of ERs populated through xn and pxn emission channels

In the ^{19}F + ^{154}Sm reaction at $E_{\text{Lab}} \approx 107$ MeV, a total of three ERs, ^{168}Lu, ^{167}Lu, and ^{167}Yb were found to be produced via xn ($x = 5, 6$) and pxn ($x = 5$) channels. These ERs populate from the excited intermediate compound system ^{173}Lu* through the entire fusion of the incident projectile ^{19}F with the ^{154}Sm target. Figures 3(a)–3(c) show the FRRDs of the ERs ^{168}Lu, ^{167}Lu, and ^{167}Yb populated through 5n, 6n, and p5n channels, respectively. As can be inferred from Figs. 3(a)–3(c), the observed mean recoil range distributions of residues ^{168}Lu, ^{167}Lu, and ^{167}Yb, show a single peak at cumulative catcher thickness $\approx$0.729, 0.749, and 0.733 mg/cm^2 in aluminium, respectively.The peak positions associated in the FRRDs of these residues (dashed curves) correspond to the entire linear momentum transfer of the projectile ^{19}F to the target ^{154}Sm. The mean ranges of ERs obtained at a depth in aluminium catcher foils are found proportional to the expected recoil range of residues in the CF of the projectile ^{19}F with target ^{154}Sm. These observations suggest the formation of ERs ^{168}Lu, ^{167}Lu, and ^{167}Yb from the excited intermediate compound system ^{173}Lu* through the entire LMT from the incident projectile ^{19}F to the ^{154}Sm target. It may therefore be inferred that these ERs are predominantly populated via the CF process only. The produced compound nucleus ^{173}Lu* may decay through the evaporation of five or six neutrons and

one proton, respectively, leaving behind the residues ^{168}Lu, ^{167}Lu, and ^{167}Yb via CF reaction. The production details of these ERs ^{168}Lu, ^{167}Lu, and ^{167}Yb can be shown as

$$^{19}\text{F} + {}^{154}\text{Sm} \Longrightarrow {}^{173}\overset{*}{\text{Lu}} \Longrightarrow {}^{173-x}\text{Lu} + x\text{n}(x = 5, 6),$$
$$\text{or} \quad \Longrightarrow {}^{172-x}\text{Yb} + \text{p}x\text{n} \ (x = 5).$$

B. FRRDs of ERs populated through αxn emission channels

In the ^{19}F + ^{154}Sm reaction at $E_{\text{Lab}} \approx 107$ MeV, a total of three ERs, namely, ^{166}Tm, ^{165}Tm, and ^{164}Tm, were observed to be populated through the αxn ($x = 3, 4, 5$) channels. These residues have the possibility of getting produced via both CF and ICF processes, which is evident from their FRRDs plots. Residues of α emission channels have multiple peaks in their FRRDs, and each peak of the FRRDs indicates a different fusion process. The contributions of different fusion processes in the population of such residues can be deduced from the area under the photo peak corresponding to particular fusion process. The degree of contribution arising from different CF and/or ICF processes varies from ER to ER, and for a specific residue it varies with the excitation energy of the compound system. The FRRDs of ERs ^{166}Tm, ^{165}Tm, and ^{164}Tm, populated via αxn ($x = 3, 4, 5$) channels reflects the interplay between CF and ICF-α processes.

(1) *CF process.* The CF process involves the fusion of ^{19}F projectile as a single entity with the ^{154}Sm target, leading to the formation of the excited compound nucleus (CN) ^{173}Lu*. The excited CN ^{173}Lu* further decays via the αxn emission channel resulting in the production of ERs ^{166}Tm, ^{165}Tm, and ^{164}Tm. Figures 4(a)–4(c) show the FRRDs of ERs $^{166-164}$Tm populated through the α emitting channels. In the measured FRRDs of the residues $^{166-164}$Tm, two distinct peaks are observed at cumulative catcher thickness $\approx$0.711, 0.756, and 0.729 mg/cm^2 and $\approx$0.482, 0.479, and 0.494 mg/cm^2, respectively in aluminium as shown in Figs. 4(a)–4(c). Here the peak at larger cumulative catcher thickness ($\approx$0.711, 0.756, and 0.729 mg/cm^2) corresponds to the recoil range of the compound system ^{173}Lu produced in CF due to entire LMT from the projectile ^{19}F to the target ^{154}Sm. Complete fusion of the incident
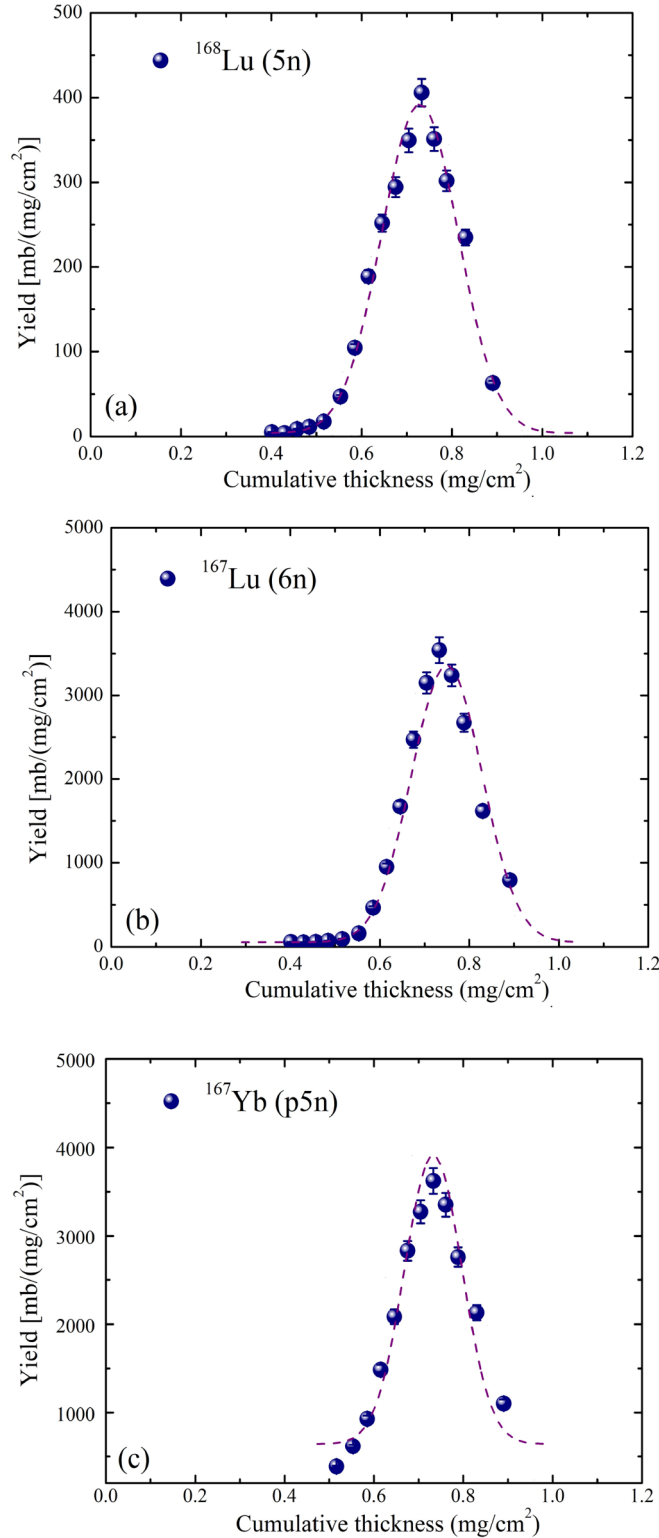
FIG. 3. Measured FRRDs for the ERs ^{168}Lu (5n), ^{167}Lu (6n), and ^{167}Yb (p5n), produced in ^{19}F + ^{154}Sm system at $E_{\text{Lab}} \approx 107$ MeV. Solid circles are the measured data and dashed lines represent the Gaussian fit to the measured FRRDs for CF of ^{19}F with ^{154}Sm.

projectile ^{19}F with the target nucleus ^{154}Sm leads to total LMT from the incident projectile to the resulting CN ^{173}Lu*. The excited CN ^{173}Lu*, on acquiring
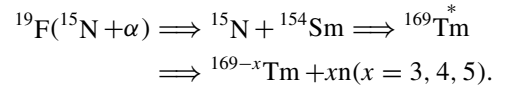
the total incident linear momentum, recoils along the beam direction up to maximum depth in the Al catcher medium. The peak at the highest recoil range in the FRRDs of ERs ^{166}Tm, ^{165}Tm, and ^{164}Tm [Figs. 4(a)–4(c)] correspond to the CF process. The production details for the formation of these ERs via CF process is given by

$$^{19}\text{F} + {}^{154}\text{Sm} \Longrightarrow {}^{173}\text{Lu}^{*}$$
$$\Longrightarrow {}^{169-x}\text{Tm} + \alpha xn \ (x = 3, 4, 5)$$
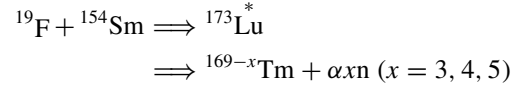
(2) *ICF-α process.* ICF-α process involves the fusion of ^{15}N, evolving from the α breakup of ^{19}F, with the ^{154}Sm target leading to the formation of IFC system ^{169}Tm*,
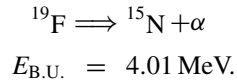
$$^{19}\text{F} \Longrightarrow {}^{15}\text{N} + \alpha$$
$$E_{\text{B.U.}} = 4.01 \, \text{MeV}.$$

The excited intermediate compound system ^{169}Tm* will further decay via the emission of xn leading to the formation of ERs $^{166-164}$Tm. Considering that incident projectile ^{19}F has α cluster structure and comprises α particle and ^{15}N, the total incident linear momentum and energy are equally distributed among the constituents α particle and ^{15}N. Thus, ^{15}N emerging from the ^{19}F through the α breakup process is associated with 15/19 p_{inc}. Hence, the residues produced via ICF-α process have a lesser recoil range in Al stopping medium due to a relatively lesser LMT in the ICF-α process as compare to CF. The ERs $^{166-164}$Tm populated through the ICF-α process may be represented as

$$^{19}\text{F}(^{15}\text{N} + \alpha) \Longrightarrow {}^{15}\text{N} + {}^{154}\text{Sm} \Longrightarrow {}^{169}\text{Tm}^{*}$$
$$\Longrightarrow {}^{169-x}\text{Tm} + xn(x = 3, 4, 5).$$

The second peak in the FRRDs of ERs $^{166-164}$Tm [Figs. 4(a)–4(c)] corresponds to the ICF-α process. Due to relatively lesser LMT, the peak corresponding to the ICF-α process in the FRRDs of $^{166-164}$Tm lies just before the peak corresponding to the CF process at smaller cumulative catcher thickness $\approx$0.482, 0.479, and 0.494 mg/cm^2, respectively.

As such, these observations indicate that the reactions ^{154}Sm (F, αxn) $^{169-x}$Tm have contributions not only from CF but also have contribution from ICF of ^{19}F (fusion of fragment ^{15}N with ^{154}Sm. In this respect, for complete fusion, the compound system ^{173}Lu decays via the statistical emission of the α-particle leaving behind the residues $^{166-164}$Tm. The same residues are also populated via incomplete fusion when the projectile ^{19}F reaches the nuclear field of the target ^{154}Sm, it breaks up into α-clusters viz. ^{4}He and ^{15}N. One of the fragments ^{15}N fuses with the target ^{154}Sm forming an IFC system ^{169}Tm* and the remnant ^{4}He (α particle) moves in the forward direction. The relative CF and ICF contributions for the ERs $^{166-164}$Tm populated via α emission channels, have been found to be $\approx$38%, 29%, 72% and $\approx$62%, 71%, and 28%, respectively, as shown in Fig. 5.
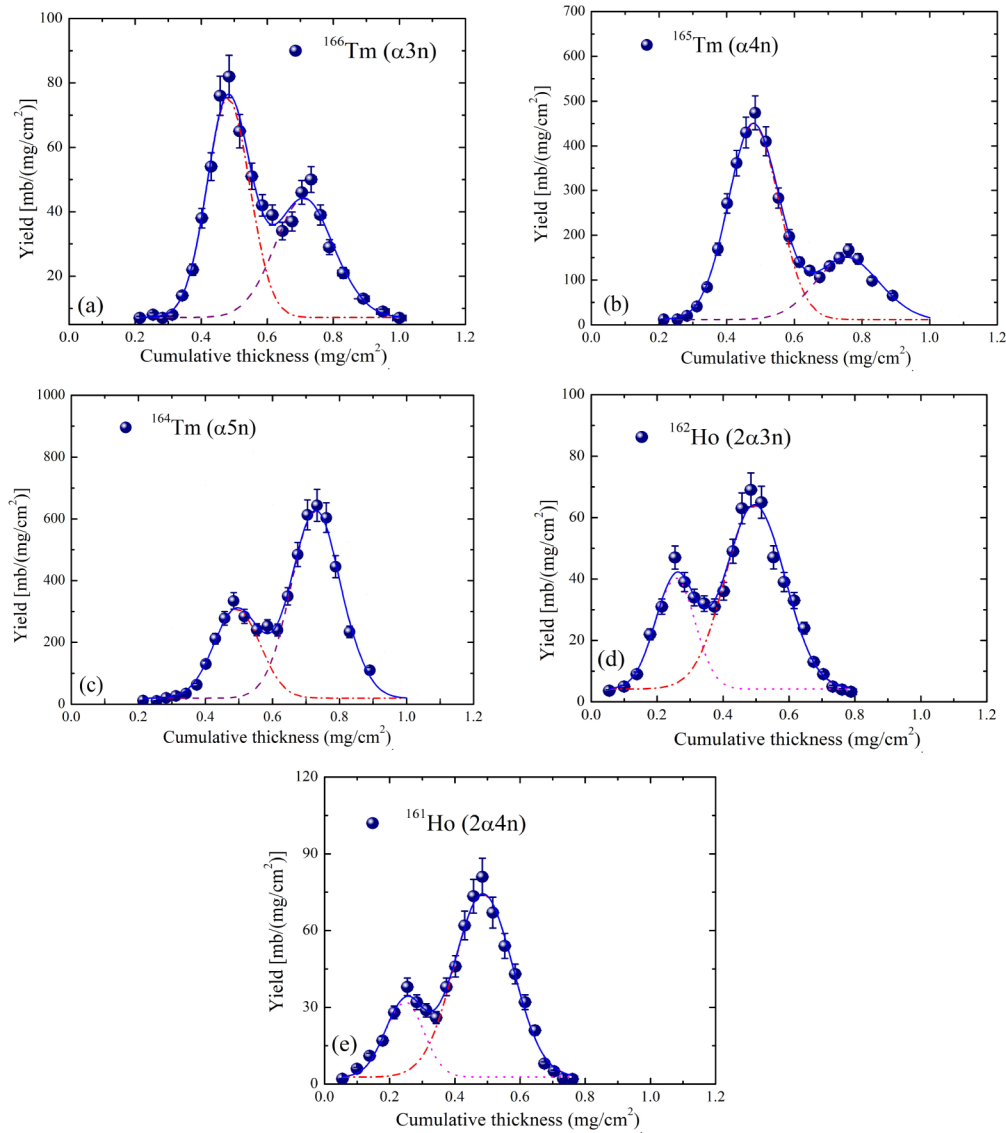
FIG. 4. Measured FRRDs for the ERs ^{166}Tm (α3n), ^{165}Tm (α4n), ^{164}Tm (α5n), ^{162}Ho (2α3n), and ^{161}Ho (2α4n), produced in ^{19}F + ^{154}Sm system at $E_{Lab} \approx 107$ MeV. Solid circles are the experimental data and dashed lines represent the Gaussian fit to the measured FRRDs for CF of ^{19}F with ^{154}Sm, while dashed-dot and dotted lines represent the Gaussian fit to the measured FRRDs for ICF-α (fusion of fragment ^{15}N) and ICF-2α (fusion of fragment ^{11}B), respectively.

C. FRRDs of ERs populated through 2αxn emission channels

In the ^{19}F + ^{154}Sm reaction at $E_{Lab} \approx 107$ MeV, a total of two ERs, namely ^{162}Ho and ^{161}Ho, were observed to be populated through the 2αxn ($x = 3$, 4) channels. ERs evolving through the 2α emitting channels have the possibility of getting populated through the CF as well as ICF processes. However, the measured FRRDs of these ERs as displayed in Figs. 4(d) and 4(e) show only two peaks, one observed at cumulative catcher thickness $\approx$0.496 and 0.487 mg/cm^2, which correspond to the mean recoil range of the ERs ^{162,161}Ho, produced by the ICF-α of ^{19}F (fusion of fragment ^{15}N with the target ^{154}Sm). The other peak at smaller cumulative catcher thickness $\approx$0.254 and 0.246 mg/cm^2 for same residues ^{162,161}Ho are associated with the mean recoil range of the ERs produced by the ICF-2α of ^{19}F (fusion of

fragment ^{11}B with the target ^{154}Sm). It was also noticed that the recoil range of the residues ^{162,161}Ho produced via the CF process which is expected at a larger range were not observed in the measured FRRDs. This shows that this reaction predominantly takes place through various modes of ICF. The FRRDs of ERs ^{162}Ho, and ^{161}Ho, populated via 2αxn ($x = 3$, 4) channels reflects the interplay between ICF-α and ICF-2α processes.

(1) *ICF-α process.* As discussed earlier, in case of ICF-α process, only 15/19 p_{inc} is transferred from the projectile ^{19}F to the resulting intermediate compound system through the fusion of ^{15}N with the ^{154}Sm target. The excited intermediate compound system ^{169}Tm* will further decay via the emission of αxn leading to the
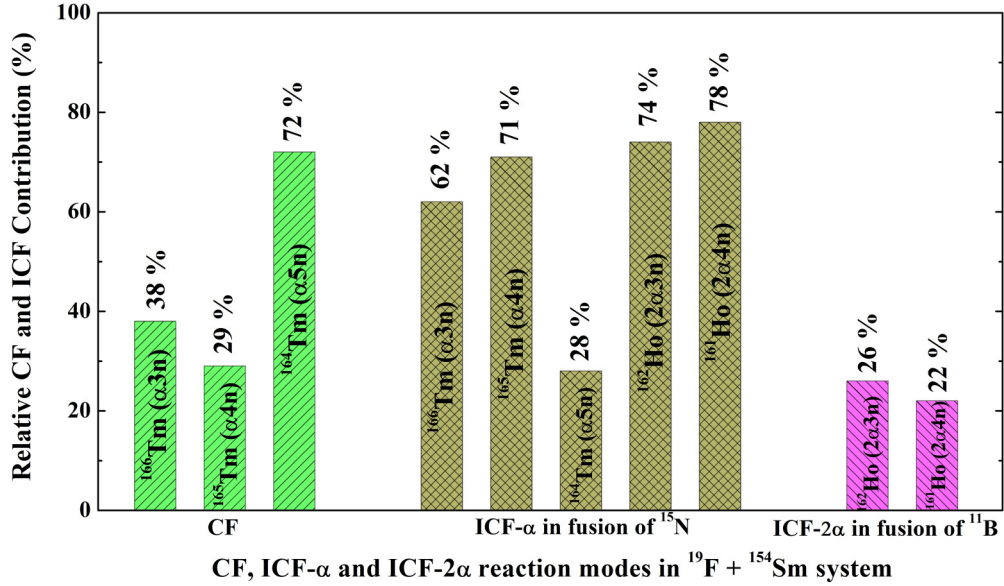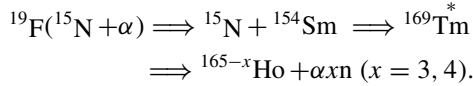
FIG. 5. Relative CF and ICF contributions of the ERs $^{166-164}$Tm (αxn), and ^{162,161}Ho ($2\alpha xn$) deduced from the measured FRRDs data for ^{19}F + ^{154}Sm system at $E_{Lab} \approx 107$ MeV.

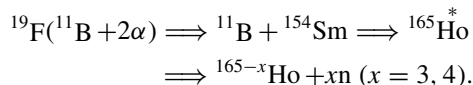formation of ERs ^{162}Ho, and ^{161}Ho. The formation of ERs ^{162,161}Ho, through the ICF-α process may be represented as

$$^{19}\text{F}(^{15}\text{N} + \alpha) \Longrightarrow {}^{15}\text{N} + {}^{154}\text{Sm} \Longrightarrow {}^{169}\text{Tm}^*$$
$$\Longrightarrow {}^{165-x}\text{Ho} + \alpha xn \ (x = 3, 4).$$

(2) *ICF-2α process.* ICF-2α process involves the fusion of ^{11}B, emerging from the 2α breakup of ^{19}F, with the ^{154}Sm target leading to the formation of IFC system ^{165}Ho*.

$$^{19}\text{F} \Longrightarrow {}^{11}\text{B} + 2\alpha$$
$$E_{\text{B.U.}} = 15.096 \, \text{MeV}.$$
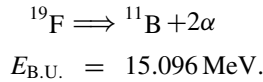
The excited intermediate compound system ^{165}Ho* will further decay via the emission of xn leading to the formation of ERs ^{162,161}Ho. Assuming that incident projectile ^{19}F has α cluster structure and comprises two α particles + ^{11}B, the total incident linear momentum and energy are equally distributed among the constituents α particles and ^{11}B. Thus, ^{11}B emerging from the ^{19}F through the 2α breakup process is endowed with 11/19 p_{inc}. Due to a relatively lesser LMT in the case of the ICF-2α process as compared to ICF-α, ERs populated through the ICF-2α process have a lesser recoil range as compared to the residues populated through the ICF-α process. The formation of ERs ^{162,161}Ho through the ICF-2α process may be represented as

$$^{19}\text{F}(^{11}\text{B} + 2\alpha) \Longrightarrow {}^{11}\text{B} + {}^{154}\text{Sm} \Longrightarrow {}^{165}\text{Ho}^*$$
$$\Longrightarrow {}^{165-x}\text{Ho} + xn \ (x = 3, 4).$$

Finally, the measured FRRDs of ERs show that the ERs ^{168}Lu, ^{167}Lu, and ^{167}Yb populated through xn/pxn emission

channels in the interaction of ^{19}F with ^{154}Sm target are produced via CF only, while the ERs $^{166-164}$Tm populated via αxn emission channels are produced via both CF and ICF processes. On the other hand, the ERs ^{162,161}Ho populated via $2\alpha xn$ emission channels are produced via ICF only.

Further, the relative ICF contributions in the fusion of fragments ^{15}N and ^{11}B with the target ^{154}Sm for the ERs ^{162,161}Ho populated via 2α emission channels, have been determined as $\approx 74\%$, 78% and $\approx 26\%$, 22%, respectively as shown in Fig. 5. The relative ICF contribution for the fusion of fragment ^{15}N with ^{154}Sm target in αxn emission channels was found to be $\approx 48\%$, while for $2\alpha xn$ emission channels it was $\approx 75\%$. Whereas the relative ICF contribution for the fusion of fragment ^{11}B with ^{154}Sm target in $2\alpha xn$ emission channels was found to be $\approx 25\%$. The present observations show that the ICF contribution due to the fusion of fragment ^{15}N is more dominant than that of the fusion of fragment ^{11}B in the present energy regime for ^{19}F + ^{154}Sm system. This can be understood on the basis of the α-breakup threshold energy ($E_{\text{B.U.}}^{\alpha}$) of the projectile. For the breakup of ^{19}F projectile into ^{4}He + ^{15}N, $E_{\text{B.U.}}^{\alpha}$ is 4.01 MeV, while in case of ^{19}F breakup into ^{8}Be + ^{11}B, $E_{\text{B.U.}}^{\alpha}$ is 15.096 MeV. The breakup of projectile ^{19}F into ^{4}He + ^{15}N is more feasible as compared to ^{8}Be + ^{11}B due to the lower value of $E_{\text{B.U.}}^{\alpha}$. Therefore, dominant contribution due to the fusion of fragment ^{15}N should be observed as compared to fusion of fragment ^{11}B with ^{154}Sm target. The same observations are also reflected in the measured FRRDs of α emission channels in the present system ^{19}F + ^{154}Sm as discussed above.

The above descriptions clearly indicate that peaks appearing at different cumulative thicknesses in the stopping medium are related to different degrees of linear momentum transfer from projectile ^{19}F to the target ^{154}Sm. The measured most probable ranges R_{Meas} deduced from FRRDs data for various residues produced through CF and ICF reactions are listed in Table II. The relative contributions of the CF and

TABLE III. Measured relative contributions of CF and ICF deduced from FRRDs curves for the ^{19}F + ^{154}Sm system at $E_{\text{Lab}} \approx 107$ MeV.

			ICF of ^{19}F	
S. No	Reactions	CF of ^{19}F	Fusion of fragment ^{15}N	Fusion of fragment ^{11}B
1.	^{154}Sm (F, 5n) ^{168}Lu	100%	–	–
2.	^{154}Sm (F, 6n) ^{167}Lu	100%	–	–
3.	^{154}Sm (F, p5n) ^{167}Yb	100%	–	–
4.	^{154}Sm (F, α3n) ^{166}Tm	38%	62%	–
5.	^{154}Sm (F, α4n) ^{165}Tm	29%	71%	–
6.	^{154}Sm (F, α5n) ^{164}Tm	72%	28%	–
7.	^{154}Sm (F, 2α3n) ^{162}Ho	–	74%	26%
8.	^{154}Sm (F, 2α4n) ^{161}Ho	–	78%	22%

ICF components are obtained by dividing the area of the corresponding peak by the total area under the observed composite FRRDs curves in Figs. 4(a)–4(e). As such the relative contributions of the CF and various ICF channels for each residue have been estimated and are listed in Table III. Finally, the total contribution of CF and ICF channels (produced via fusion of projectile fragments ^{15}N, and ^{11}B with the target ^{154}Sm) at $E_{\text{Lab}} \approx 107$ MeV has been evaluated as 78%, 19%, and 3%, respectively.

The range integrated cross sections (σ_{FRRD}) for the identified ERs were deduced using the standard formalism [22]. In order to compare the range integrated yields of ERs produced via CF and/or ICF, the statistical model (SM) calculations were done using the code PACE-4 [40,41]. The code PACE-4 is based on the Hauser-Feshbach formalism of CN decay [42]. This code takes into account the statistically equilibrated emission of light particles (i.e., neutron, proton, and α particle, etc.) and γ rays, only for the decay of the CN. The possibility of ICF, and/or pre-equilibrium emission are not considered in this code. Level density parameter a ($= A/K$) MeV^{-1} is an important parameter for the calculation of cross section, where A is the mass number of the CN and K is the level density parameter constant. In the present work, for the ^{19}F + ^{154}Sm system, $K = 10$ has been taken in the PACE-4 calculations. More details about the analysis of data using PACE-4 code is given in our previous work [14].

The CF of ^{19}F with ^{154}Sm followed by the evaporation of 1 proton and 5 neutrons from the CN ^{173}Lu* leads to the production of ER ^{167}Yb. The residual nucleus ^{167}Yb decays to ^{167}Tm by electron capture (EC) and has been identified by 114 and 176 keV γ ray. The same residue may also be populated by EC and/or β^+ decay of its higher charge precursor isobar ^{167}Lu produced via the reaction ^{154}Sm (F, 6n) ^{167}Lu. The half-life of precursor (i.e., ^{167}Lu $\rightarrow t_{1/2}^{\text{pre}} = 51.5$ min) is larger than the half-life of the daughter nuclei (i.e., ^{167}Yb $\rightarrow t_{1/2}^{d} = 17.5$ min). In this case, the independent production cross section ($\sigma_{\text{indp}}^{\text{Meas}}$) of ^{165}Yb has been deduced using the following successive radio-active decay formulations [43],

$$N_d(t) = C_{t=0} \times e^{-\lambda_d t} + \frac{(P_{\text{pre}}.\lambda_{\text{pre}})}{\lambda_d - \lambda_{\text{pre}}} \times N_{\text{pre}}(t).e^{-\lambda_{\text{pre}}.t}, \quad (3)$$

where $N_d(t)$ and $N_{\text{pre}}(t)$ are the number of daughter and precursor nuclei produced at time t. $C_{t=0}$ is the number of cumulative (precursor + daughter) nuclei produced at the end

of the irradiation, and λ_{pre} and λ_d are the decay constants of precursor and daughter nuclei, respectively. The value of $N_{\text{pre}}(t)$ has been deduced from the measured decay curve analysis of the ER ^{167}Lu. The value of $N_d(t)$ for ER ^{167}Yb has been obtained by solving Eq. (3), which has been translated to its production cross section ($\sigma_{\text{indp}}^{\text{Meas}}$).

Further, CF of ^{19}F with ^{154}Sm followed by emission of α particle and four neutrons leads to production of ER ^{165}Tm. The same ER may also be formed by ICF process. The residue ^{165}Tm, with half-life 30.06 h that decays to ^{165}Er, has been identified by γ rays of 243, and 297 keV energy. The residue ^{165}Tm produced via the reaction ^{154}Sm (F, α4n) ^{165}Tm may also be populated by the EC and/ or β^+ decay of the higher charge precursor isobars ^{165}Lu and ^{165}Yb. Hence, the measured cumulative cross sections of ^{165}Tm may have contributions from the decay of precursor isobars of ^{165}Lu and ^{165}Yb produced in 8n and p7n emission channels of the CF in addition to direct production of ^{165}Tm. In this case, the half-life of precursor (i.e., ^{165}Yb $\rightarrow t_{1/2}^{\text{pre}} = 9.9$ min) is smaller than the daughter nuclei (i.e., ^{165}Tm $\rightarrow t_{1/2}^{d} = 30.06$ h). As demonstrated by Cavinato et al. [44], the independent production cross section (σ_{ind}) of the daughter nuclei may be defined in terms of cumulative (σ_{cum}) and precursor (σ_{pre}) cross section as follows;

$$\sigma_{\text{ind}} = \sigma_{\text{cum}} - P_{\text{pre}}.\frac{t_{1/2}^{d}}{t_{1/2}^{d} - t_{1/2}^{\text{pre}}}.\sigma_{\text{pre}} \quad (4)$$

Here P_{pre} is the branching ratio of precursor decay to the final nucleus. The contribution due to the decay of precursor isobar ^{165}Yb to the ER ^{165}Tm has been separated from cumulative contribution to get the independent yield for the production of ^{165}Tm by using the expression (5) based on Cavinato et al. [44],

$$\sigma_{\text{ind}}(^{165}\text{Tm}) = \sigma_{\text{cum}} - 1.0055.\sigma_{\text{pre}}. \quad (5)$$

The range integrated cross sections (σ_{FRRD}) along with PACE-4 predictions ($\sigma_{\text{PACE}-4}$) for the identified ERs are listed in Table IV. It was observed that the contribution of CF channels (xn/pxn emission channels) satisfactorily matches with PACE-4 predictions. However, the contribution of ICF channels (αxn and 2αxn emission channels) could not be reproduced by PACE-4 predictions using the same set of parameters, since, PACE-4 code does not take into account ICF

TABLE IV. Measured range integrated cross sections (σ_{FRRD}) and their errors deduced from FRRDs data along with PACE-4 calculations ($\sigma_{\text{PACE}-4}$) for the $^{19}\text{F} + ^{154}\text{Sm}$ system at $E_{\text{Lab}} \approx 107$ MeV.

S. No.	Residues	σ_{FRRD} (mb)	$\sigma_{\text{PACE}-4}$ (mb)
1	^{154}Sm (F, 5n) ^{168}Lu	78.9 ± 11.1	71.1
2	^{154}Sm (F, 6n) ^{167}Lu	543.7 ± 76.2	565
3	^{154}Sm (F, p5n) ^{167}Yb	87.4 ± 12.3	81.5
4	^{154}Sm (F, α3n) ^{166}Tm	26.9 ± 5.2	1.1
5	^{154}Sm (F, α4n) ^{165}Tm	97.8 ± 18.5	32.4
6	^{154}Sm (F, α5n) ^{164}Tm	132.1 ± 27.4	52.3
7	^{154}Sm (F, 2α3n) ^{162}Ho	19.4 ± 3.9	1.1
8	^{154}Sm (F, 2α4n) ^{161}Ho	13.6 ± 2.9	–

contribution. Nevertheless, it may be noted that the measured FRRDs of the identified residues $^{166-164}\text{Tm}$, ^{162}Ho, and ^{161}Ho provide the experimental evidence of breakup of projectile ^{19}F in interaction with ^{154}Sm the measured energy range. The measured FRRDs of these ERs clearly indicate the signature of α clustering in ^{19}F nuclei.

In the present FRRDs measurements, the activation technique was used for the identification of ERs populated. However, some of the ERs may not be detected owing to very long or short half-lives or no intense γ rays due to the limitation of this method. The cross sections of such ERs were incorporated using the statistical model code PACE-4. The branching of the sum of the measured channels, i.e., ($\sigma_{xn+pxn}^{\text{Expt}}$) with respect to the complete fusion (σ_{CF}) at $E_{\text{Lab}} \approx 107$ MeV has been calculated using the PACE-4. The theoretical ratio of combined cross sections of these channels to the complete fusion $R_{\sigma}^{\text{Theo}}(= \sigma_{xn/pxn}/\sigma_{\text{CF}})$ is calculated for the $^{19}\text{F} + ^{154}\text{Sm}$ system. The neutron and/or proton evaporation channels are found to be dominant for the measured energy. The combined cross section of xn/pxn channels is found to be 91% of CF in the system $^{19}\text{F} + ^{154}\text{Sm}$ at $E_{\text{Lab}} \approx 107$ MeV. The remaining contributions are mostly from the charged particle evaporation channels which are difficult to extract from the measured γ lines as they are contaminated by the contributions from the transfer/ICF channels. In this respect, the experimental CF cross sections were calculated as $\sigma_{\text{CF}}^{\text{Expt}} = \sigma_{xn+pxn}^{\text{Expt}}/R_{\sigma}^{\text{Theo}}$ [45]. Hence, $\sigma_{\text{CF}}^{\text{Expt}}$ the corrected total measured CF cross section, including contributions from all the observed and missing CF channels.

The ICF contribution in all α emission channels has been deduced adopting the standard procedure [17–20]. The ICF cross sections ($\sigma_{\text{ICF}}^{\text{Expt}}$) for the ERs were deduced by subtracting the PACE-4 cross sections from the measured cross sections at studied energy. Then, the ICF probability function, S_{ICF}, which is a measure of the strength of ICF, has been deduced using the following expression:

$$S_{\text{ICF}}(\%) = \frac{\sigma_{\text{ICF}}^{\text{Expt}}}{\sigma_{\text{CF}}^{\text{Expt}} + \sigma_{\text{ICF}}^{\text{Expt}}} \times 100. \qquad (6)$$

It is important to mention that the quantity S_{ICF} is not based only on experimental evidences and for obvious technical reasons, the code PACE-4 has also been used in its deduction.

The S_{ICF} value deduced from the present FRRDs measurements for the $^{19}\text{F} + ^{154}\text{Sm}$ system at $E_{\text{Lab}} \approx 107$ MeV was found to be 21%, which is in agreement with those obtained from the excitation functions measurements for the same system at similar energy range [46].

IV. SUMMARY AND CONCLUSIONS

The role of partial linear momentum transfer on incomplete fusion dynamics was studied through the measurements of FRRDs of the evaporation residues populated in $^{19}\text{F} + ^{154}\text{Sm}$ system at $E_{\text{Lab}} \approx 107$ MeV. The FRRDs of eight ERs, namely, ^{168}Lu (5n), ^{167}Lu (6n), ^{167}Yb (p5n), ^{166}Tm (α3n), ^{165}Tm (α4n), ^{164}Tm (α5n), ^{162}Ho (2α3n), and ^{161}Ho (2α4n) were determined in this measurement. The FRRD of ERs produced through the xn and pxn channels comprises a single peak only, suggesting transfer of entire linear momentum from the incident projectile ^{19}F to the resulting compound system $^{173}\text{Lu}^*$ through the CF process. On the other hand, the analysis of measured FRRDs inferred that the ERs populated through α emitting channels includes multiple component of linear momentum transfer from the ^{19}F projectile to the ^{154}Sm target. Different partial linear momentum transfer components were attributed to the fusion of ^{15}N and/or ^{11}B from the projectile ^{19}F to the target nucleus ^{154}Sm. The relative contribution of the components produced via complete and/or incomplete fusion channels in the production of individual residues was obtained. It was found that, in general, the residues are not only populated via complete fusion but incomplete fusion also plays an important role in the production of various reaction products involving direct α cluster emission at the present energy. Present FRRDs data clearly shows that the residues ^{168}Lu, ^{167}Lu, and ^{167}Yb are produced through complete fusion while the residues ^{166}Tm, ^{165}Tm, and ^{164}Tm are produced via the incomplete fusion channel also. It is also inferred that measurements are consistent with ICF reaction hypothesis of break-up fusion model wherein fusion of projectile fragments (in its breakup) takes place with the target nucleus. In the measured FRRDs of residues ^{162}Ho, and ^{161}Ho, the absence of the peak corresponding to the complete fusion channel indicates that the population of these ERs has taken place mainly via various incomplete fusion channels. The analysis of present FRRDs data inferred that the ICF contribution due to the fusion of fragment ^{15}N is more dominant than that of the fusion of fragment ^{11}B with ^{154}Sm target. Further, the total contribution of CF and ICF channels (produced via fusion of projectile fragments ^{15}N, and ^{11}B with the target ^{154}Sm) at $E_{\text{Lab}} \approx 107$ MeV has been evaluated as 78%, 19%, and 3%, respectively. The FRRDs peaks of α emission channels at smaller distances clearly show an experimental signature of the breakup of the ^{19}F projectile (into $\alpha + ^{15}\text{N}$ or $2\alpha + ^{11}\text{B}$). Hence, the measured FRRDs clearly provide an evidence of the presence of α clustering in ^{19}F nuclei. The incomplete fusion strength function (S_{ICF}) was deduced from the measured FRRDs data for the present $^{19}\text{F} + ^{154}\text{Sm}$ system and found to be 21%, which is in good agreement with those obtained from the excitation functions measurements for the same system in similar energy regime [46].

The present study also highlights that the $N \neq Z$ α clustered projectiles (like ^{19}F) have significant contributions of ICF on fusion cross sections at above barrier energies. However, the ICF probability for the $N \neq Z$ α clustered projectiles is found to be smaller than the $N = Z$ α clustered projectile with similar $E_{\mathrm{B.U.}}^{\alpha}$ values.

ACKNOWLEDGMENTS

[1] H. C. Britt and A. R. Quinton, Phys. Rev. **124**, 877 (1961).

[2] R. G. Stokstad, Y. Eisen, S. Kaplanis, D. Pelte, U. Smilansky, and I. Tserruya, Phys. Rev. Lett. **41**, 465 (1978).

[3] L. C. Vaz, J. M. Alexander, and G. R. Satchler, Phys. Rep. **69**, 373 (1981).

[4] J. R. Leigh, M. Dasgupta, D. J. Hinde, J. C. Mein, C. R. Morton, R. C. Lemmon, J. P. Lestone, J. O. Newton, H. Timmers, J. X. Wei, and N. Rowley, Phys. Rev. C **52**, 3151 (1995).

[5] L. Zhu, J. Su, W.-J. Xie, and F.-S. Zhang, Nucl. Phys. A **915**, 90 (2013).

[6] B. K. Nayak, R. K. Choudhury, A. Saxena, P. K. Sahu, R. G. Thomas, D. C. Biswas, B. V. John, E. T. Mirgule, Y. K. Gupta, M. Bhike, and H. G. Rajprakash, Phys. Rev. C **75**, 054615 (2007).

[7] X. Bao, S. Guo, H. Zhang, and J. Li, J. Phys. G: Nucl. Part. Phys. **43**, 125105 (2016).

[8] G. Royer and C. Piller, J. Phys. G: Nucl. Part. Phys. **18**, 1805 (1992).

[9] J. X. Wei, J. R. Leigh, D. J. Hinde, J. O. Newton, R. C. Lemmon, S. Elfstrom, J. X. Chen, and N. Rowley, Phys. Rev. Lett. **67**, 3368 (1991).

[10] D. J. Hinde, M. Dasgupta, J. R. Leigh, J. P. Lestone, J. C. Mein, C. R. Morton, J. O. Newton, and H. Timmers, Phys. Rev. Lett. **74**, 1295 (1995).

[11] D. J. Hinde, M. Dasgupta, J. R. Leigh, J. C. Mein, C. R. Morton, J. O. Newton, and H. Timmers, Phys. Rev. C **53**, 1290 (1996).

[12] K. Siwek-wilczyńska, A. Borowiec, I. Skwira-Chalot, and J. WilczyÂ´nski, Int. J. Mod. Phys. E **17**, 12 (2008).

[13] H. Kumar, S. A. Tali, M. A. Ansari, D. Singh, R. Ali, K. Kumar, N. Sathik, A. Ali, S. Parashari, R. Dubey *et al.*, Eur. Phys. J. A **54**, 47 (2018).

[14] A. Mahato, D. Singh, P. K. Giri, S. B. Linda, H. Kumar, S. A. Tali, M. A. Ansari, R. Kumar, S. Muralithar, and R. P. Singh, Eur. Phys. J. A **56**, 131 (2020).

[15] D. Pierroutsakou, M. Di Toro, F. Amorini, V. Baran, A. Boiano, A. De Rosa, A. D'Onofrio, G. Inglima, M. La Commara, A. Ordine *et al.*, Eur. Phys. J. A **16**, 423 (2003).

[16] H. Morgenstern, W. Bohne, W. Galster, K. Grabisch, and A. Kyanowski, Phys. Rev. Lett. **52**, 1104 (1984).

[17] D. Singh, R. Ali, M. Arzal Ansari, B. S. Tomar, M. H. Rashid, R. Guin, and S. K. Das, Phys. Rev. C **83**, 054604 (2011).

[18] S. Ali, T. Ahmad, K. Kumar, M. Gull, I. A. Rizvi, A. Agarwal, S. S. Ghugre, A. K. Sinha, and A. K. Chaubey, Eur. Phys. J. A **54**, 56 (2018).

[19] S. A. Tali, H. Kumar, M. A. Ansari, A. Ali, D. Singh, R. Ali, P. K. Giri, S. B. Linda, R. Kumar, S. Parashari, S. Muralithar, and R. P. Singh, Phys. Rev. C **100**, 024622 (2019).

[20] D. Singh, R. Ali, M. A. Ansari, B. S. Tomar, M. H. Rashid, R. Guin, S. K. Das, R. Kumar, R. P. Singh, S. Muralithar, and R. K. Bhowmik, Pramana J. Phys. **82**, 683 (2014).

[21] M. Gull, K. Kumar, S. Ali, T. Ahmad, S. Dutt, I. A. Rizvi, A. Agarwal, and R. Kumar, Phys. Rev. C **98**, 034603 (2018).

[22] P. K. Giri, A. Mahato, D. Singh, S. B. Linda, H. Kumar, S. A. Tali, M. A. Ansari, R. Kumar, S. Muralithar, and R. P. Singh, Phys. Rev. C **100**, 054604 (2019).

[23] M. La Cognata, M. Fisichella, A. Di Pietro, P. Figuera, V. Z. Goldberg, S. Cherubini, J. P. Fernández Garcia, M. Gulino, L. Lamia, D. Lattuada *et al.*, Phys. Rev. C **99**, 034301 (2019).

[24] R. Otani, R. Kageyama, M. Iwasaki, M. Kudo, M. Tomita, and M. Ito, Phys. Rev. C **90**, 034316 (2014).

[25] S. Ohkubo and Y. Ishikawa, Phys. Rev. C **31**, 1560 (1985).

[26] P. Descouvemont and D. Baye, Nucl. Phys. A **463**, 629 (1987).

[27] T. Sakuda and F. Nemoto, Prog. Theor. Phys. **62**, 1274 (1979).

[28] F. Nemoto and H. Bando, Prog. Theor. Phys. **47**, 1210 (1972).

[29] D. Torresi, C. Wheldon, T. Kokalova, S. Bailey, A. Boiano, C. Boiano, M. Fisichella, M. Mazzocco, C. Parascandolo, D. Pierroutsakou *et al.*, Phys. Rev. C **96**, 044317 (2017).

[30] S. Wilmes, V. Wilmes, G. Staudt, P. Mohr, and J. W. Hammer, Phys. Rev. C **66**, 065802 (2002).

[31] P. K. Giri, A. Mahato, D. Singh, S. B. Linda, S. R. Abhilash, N. K. Deb, G. R. Umapathy, S. Ojha, D. Kabiraj, and S. Chopra, Ind. J. Pure App. Phys. **57**, 675 (2019).

[32] M. Thakur, R. Dubey, S. R. Abhilash, B. R. Behera, B. P. Mohanty, D. Kabiraj, S. Ojha, and H. Duggal, Methods X **3**, 542 (2016).

[33] The Stopping and Range of Ions in Matter (SRIM-2008.04) http://www.srim.org/.

[34] B. Wilken and T. A. Fritz, Nucl. Instrum. Methods **138**, 331 (1976).

[35] E. T. Subramaniam, B. P. Ajith Kumar, R. K. Bhowmik, http://www.iuac.res.in/NIAS.

[36] S. Y. F Chu, L. P. Ekstrom, and R. B. Firestone, The Lund/LBNL Nuclear Data Search (LBNL, Berkeley, USA, Version 2.0 (1999).

[37] National Nuclear Data Centre, Brookhaven National Laboratory.

[38] M. A. Ansari, R. K. Y. Singh, M. L. Sehgel, V. K. Mittal, D. K. Avasthi, and I. M. Govil, Ann. Nucl. Energy **11**, 607 (1984).

[39] D. J. Parker, J. J. Hogan, and J. Asher, Phys. Rev. C **35**, 161 (1987).

[40] A. Gavron, Phys. Rev. C **21**, 230 (1980).

[41] O. B. Tarasov and D. Bazin, Nucl. Instrum. Methods B **266**, 4657 (2008).

[42] W. Hauser and H. Feshbach, Phys. Rev. **87**, 366 (1952).

[43] R. D. Evans, *The Atomic Nucleus* (McGraw–Hill, New York, 1982).

[44] M. Cavinato, E. Fabrici, E. Gadioli, E. Gadioli Erba, P. Vergani, M. Crippa, G. Colombo, I. Redaelli, and M. Ripamonti, Phys. Rev. C **52**, 2577 (1995).

[45] C. S. Palshetkar, S. Santra, A. Chatterjee, K. Ramachandran, Shital Thakur, S. K. Pandit, K. Mahata, A. Shrivastava, V. V. Parkar, and V. Nanal, Phys. Rev. C **82**, 044608 (2010).

[46] A. Mahato, D. Singh, N. Sharma, P. K. Giri, S. B. Linda, H. Kumar, S. A. Tali, M. A. Ansari, A. Ali, N. K. Deb, N. P. M. Sathik, S. Kumar, R. Kumar, S. Muralithar, and R. P. Singh, Phys. Rev. C **106**, 014613 (2022).